Eur. Phys. J. Plus (2021) 136:333
https://doi.org/10.1140/epjp/s13360-021-01307-0

THE EUROPEAN PHYSICAL JOURNAL PLUS

Regular Article

# Entropy generation analysis in a single-turn pulsating heat pipe considering phase change modeling

**Farrokh Mobadersani**[1,a], **Araz Rezavand Hesari**[2]

[1] Department of Mechanical Engineering, Urmia University of Technology, Urmia, Iran
[2] Department of Mechanical Engineering, Université Laval, Québec, Canada

Received: 1 January 2021 / Accepted: 13 March 2021


**Abstract** Pulsating heat pipes are one of the most important solutions for the daily increasing demand for high-performance cooling systems. Despite numerous studies in this field, most of the previous works, including experimental and numerical studies, take constant heat flux boundary condition into account and neglect thin-film boiling and condensation. Furthermore, an improvement in accuracy is essential for the models that consider constant temperature boundary condition. In order to satisfy the essence of accuracy improvement in modeling of constant temperature boundary condition PHPs, the present study models a single-turn pulsating heat pipe numerically, which is based on the best predictor correlations for flow boiling and condensation. Moreover, a thin liquid film is considered in the calculation of mass transfer from vapor plugs, because of annular flow assumption. All fundamental equations, except liquid-slug-energy equation, are solved explicitly. Comparison of displacement of the liquid slug, with the previous works, indicates an increase in both amplitude and frequency. In contrast to the previous mathematical models, acceptable agreement between empirical data and the present mathematical model has been demonstrated. Furthermore, entropy generation analysis has been carried out to achieve optimum operating conditions and the results have been presented for different pipe diameters. These data also depict the effect of diameter on the properties of PHP, besides entropy generation analysis. Bejan number for simulations has been derived to show heat transfer share in entropy generation. It is shown that the share of heat transfer in entropy generation also increases by the diameter.

## List of symbols

| | |
|---|---|
| $A$ | Section area ($m^2$) |
| Ca | Capillary number, $\mu v_{ls}/\sigma$ |
| $C_{li}$ | Friction factor for liquid, $C_{li} = 16$ |
| $c_p$ | Specific heat (J/Kg K) |
| $c_v$ | Specific heat (J/Kg K) |
| $C_v$ | Friction factor for liquid, $C_v = 0.046$ |
| $d$ | Diameter, (m) |
| $E$ | Sensible heat corrector factor |

[a] emails: f.mobadersani@mee.uut.ac.ir; fmobadersani@gmail.com (corresponding author)

| | |
|---|---|
| $f$ | Friction factor |
| $g$ | Gravitational acceleration, (m/s$^2$) |
| $G$ | Mass flux, (Kg/m$^2$.s) |
| $h$ | Specific enthalpy, (J/Kg) |
| $h_{fg}$ | Phase change enthalpy, (J/Kg) |
| $H_{l\text{sen}}$ | Sensible heat coefficient, (W/m$^2$ K) |
| Ja | Jacob number, $\text{Ja} = h_{fg}/\left(c_p \cdot \Delta T_{\text{sat}}\right)$ |
| $K$ | Turn pressure loss coefficient |
| Ka | Karman number, $\text{Ka} = f \cdot \text{Re}^2$ |
| $L$ | Length, (m) |
| $L_e$ | Evaporator length, (m) |
| $L_c$ | Condenser length, (m) |
| $m$ | Mass, (Kg) |
| $\dot{m}$ | Mass flow rate, (Kg/s) |
| $N_t$ | Number of turns |
| $P$ | Pressure, (Pa) |
| PHP | Pulsating heat pipe |
| Pr | Prandtl number |
| $Q$ | Heat rate, (W) |
| $q''$ | Heat flux, (W/m$^2$) |
| $R$ | Gas constant, (J/Kg K) |
| Re | Reynolds number |
| $r_t$ | Turn radius, (m) |
| $S$ | Entropy, (J/K) |
| $\dot{S}$ | Entropy generation (W/K) |
| $\dot{S}'$ | Entropy generation at length unit (W/K m) |
| $t$ | Time (s) |
| $T$ | Temperature, (K) |
| $T_L$ | Wall temperature, (K) |
| $T_w$ | Temperature of the liquid slug (K) |
| $u$ | Specific internal energy, (J/Kg) |
| $V$ | Volume, (m$^3$) |
| $v_{\text{ls}}$ | Liquid slug velocity, (m/s$^2$) |
| $x$ | Distance, (m) |
| $x_q$ | Vapor quality |
| $X_{tt}$ | Lockhart–Martinelli parameter |
| $We$ | Weber number |

**Greek symbols**

| | |
|---|---|
| $\alpha$ | Thermal diffusivity (m$^2$/s) |
| $\mu$ | Viscosity (Pa s) |
| $\rho$ | Density (Kg/m$^3$) |
| $\sigma$ | Surface tension (N/m) |
| $\tau$ | Shear stress (Pa) |
| $\eta$ | Boiling heat transfer corrector |
| $\delta$ | Thickness (m) |

**Subscripts**

| | |
|---|---|
| film | Liquid film |
| *F* | Flow |
| gen | Generation |
| *l* | Liquid |
| Late | Latent |
| li | Ith liquid slug |
| ls | Liquid slug |
| Sen | Sensible |
| sp | Single phase |
| *T* | Total |
| Th | Thermal |
| tot | Total |
| tp | Two-phase |
| *v* | Vapor |
| vl | Left vapor |
| vr | Right vapor |
| *W* | Wall |

## 1 Introduction

Advances in electronic devices and increase in their performance have provided a high demand for thermal management of such devices, and this has turned into one of the most challenging problems. Size, power consumption, and heat transfer capacity are important characteristics that are of very high demand in such cooling devices. Various methods have been proposed as solutions by many researchers [1–7]. In 1990s Akachi introduced a new, two-phase heat exchanger with no power consumption. PHPs are composed of evaporator and condenser sections and heat transfer from high-temperature source to low-temperature source is accomplished through oscillatory motion of the working fluid. PHPs are one or multi-bend capillary tubes with liquid slugs and vapor plugs. Small size and no power consumption besides its high heat transfer capabilities have made PHPs very appealing heat transfer devices. They are classified into two categories, namely closed looped pulsating heat pipes (CLPHP) and open loop pulsating heat pipes (OLPHP). Increased demand for cooling requires optimization and performance increase of PHPs. This brings in the requirement for more comprehensive studies and better models to investigate their operation and get a clear understanding of their work and details of heat transfer mechanisms involved in them. For these reasons, many numerical and experimental studies have been conducted on this subject. It is worth mentioning that pulsating flows have recently attracted a lot of attention [8–12]. Some researchers have reviewed and summarized the important numerical and experimental works done on PHPs [13, 14].

Consideration of liquid film's meniscus region was applied in the study of Zhang et al. [15, 16], which showed a reduction of the oscillation amplitude due to pipe diameter and evaporator temperature decrease. However, the frequency of oscillations increased insignificantly. Lenhard et al. [17] modeled pulsating heat pipes using CFD software (ANSYS FLUENT) to investigate the heat transfer in the evaporator and condenser. Their model shows how geometric changes affect behavior of the pulsating heat pipes and how much heat output can be transferred by it. A simple model consisting of mass, momentum and energy equations

has been presented by Zhang et al. [16] and their non-dimensional form has been obtained for a single-turn PHP. This study suggests that angular frequency and oscillation amplitude are not significantly affected by gravity and initial displacement of the liquid slug. In the study of Ayel et al. [18], a flat plate pulsating heat pipe is used to visualize the flow patterns under various gravity levels. To investigate the effects of different liquid properties on a simple geometry, Mameli et al. [19] performed thermal simulations for a pulsating heat pipe, considering constant heat flux boundary condition. They did not model film boiling and condensation and accounted only for the thermodynamic properties of the film. Their results are presented using thermal resistance. Mohammadi et al. [20] experimentally studied a ferrofluidic closed-looped pulsating heat pipe. They showed that the use of ferrofluid improves thermal performance and reduces thermal resistance. Experimental study of constant heat flux, closed looped pulsating heat pipes with liquid hydrogen as the working fluid is presented by Gan et al. [21] for different adiabatic lengths. It is observed in their study that as the heat load increases, stable temperature profiles are maintained. Thermal resistance is larger for a longer adiabatic length, but the values remain almost constant. Visualization studies of flow pattern and circulation in closed loop PHPs have also been performed [22, 23].

The thermal characteristics of silicon-based micro-PHP were experimentally studied by Youn and Kim [24] and Qu et al. [25], measuring various filling ratios, inclination angles, and heat inputs. A single-turn PHP has been modeled by Ma et al. [26], assuming the thermal energy as the driving force of the liquid slug. The effects of pipe characteristics and filling ratio on the frequency and amplitude of liquid slug were studied in this work. Their model neglects film boiling and condensation. The effects of multiple heat sources on the performance of closed-loop pulsating heat pipes are demonstrated by the experimental study of Kammuange-Lue et al. [27]. Constant heat flux boundary condition is maintained in this work. Performance of U-shaped PHPs with fixed temperature boundary conditions is numerically investigated by Arabnejad et al. [28]. The results show that heat transfer rate due to convection and boiling increases as evaporator temperature increases. This is due to the higher pulse amplitude and frequency. The data from this study show that the share of boiling heat transfer is larger than sensible heat transfer. This is in contrast with all the previous studies. Inaccurate assumptions seem to be the reason for this discrepancy between this study and other works. Sakulchangsatjatai et al. [29] constructed a mathematical modeling of closed loop PHP with bottom heat mode. Their study showed that in bottom heat mode, the maximum heat transfer rate can be achieved by the highest evaporator temperature.

A correlation to predict input heat flux is proposed by Shafii et al. [30] through their experimental study of PHPs. In experimental investigation of a vertical closed-loop pulsating heat pipe by Kammunaug-Lue [31], a correlation is proposed to predict the maximum heat flux. Kumar et al. [32] experimentally studied the effects of surface tension variation of the working fluid for constant heat flux evaporator section. Their study demonstrates that lower surface tension results in minimum evaporation temperature and thus lowest thermal resistance in the vertical orientation, while surface tension does not have an appreciable effect on the performance in horizontal position.

Optimal operation conditions for heat transfer devices can be achieved by investigation of the second law of Thermodynamics. This is a very helpful technique that studies the entropy in PHP. Heat transfer, irreversible processes, and fluid flow generate entropy in the PHP. Performing entropy generation studies for different case studies has attracted a lot of attention, and many scientists have used it in their works.

Effects of Reynolds number and wall temperature on the entropy distribution of the pipe system have been analyzed by Al-Zaharnah [33]. For different wall temperatures, the influence of fluid viscosity on entropy generation has been studied by Al-Zaharnah and Yilbas

[34]. It revealed that the rate of entropy generation increases due to high wall-temperature of the pipe. Taghilou et al. [35] conducted a study for optimization of double pipe heat exchanger, in which minimization of the entropy generation in the heat exchanger has been analyzed. The results show that entropy generation, manufacturing costs and pumping power reduce in all conditions. For a circular tube with baffle, the effect of fluid flow geometry parameters on the entropy generation has been examined by Tandiroglu [36]. This paper has calculated the average time of the entropy generation corresponding to fluid flow geometry parameters with constant heat flux condition. The impact of the transverse magnetic field on the entropy generation due to mixed convection between two isothermal cylinders has been studied by Mahian et al. [37]. The entropy generation and Bejan number are investigated for different values of the Hartmann number, radius ratios, and a flow parameter. It is concluded that increase in magnetic field decreases the entropy generation, whereas the impact of MHD flow on the entropy generation reduces with a decrease in the radius ratios.

Entropy generation analysis in an un-looped PHP, containing water as the working fluid, has been investigated by Jafarmadar et al. [38]. The pressure loss at the bends of PHP and thin-film boiling and condensation have been neglected in their study. Although the entropy generation has been reported in each cycle of PHP operation in the study, they concluded that using PHP is not reasonable in small pipe diameters.

Most of the published articles on pulsating heat pipes are restricted to the CFD-based numerical analysis or experimental investigations. On the other hand, in most of the mathematically formulated studies, the phase change phenomena (liquid to vapor phase and vice-versa) are neglected. This neglection may result in missing the actual nature of pulsating heat pipes' operation. On the other hand, despite the importance of entropy generation and second law analysis in optimization, little attention has been given to this analysis in pulsating heat pipes. In the present study, the entropy generation due to evaporation and condensation mechanisms in a pulsating heat pipe is studied by mathematical modeling of PHP operation using the most accurate phase change correlations in the literature. This brings the error of the calculations into a minimum.

## 2 Mathematical modeling

In this paper the operation of a single-turn, U-shaped OLPHP has been studied. Previous works have demonstrated that the behavior of multi-turn PHPs can be modeled by single-turn U-shaped pipe [23, 39]. As shown in Fig. 1, the simple structure of U-shaped open loop PHP used in this study consists of a liquid slug, with two neighboring vapor plugs. The liquid slug, left and right-hand side position of which are $x_l$ and $x_r$, respectively, oscillates between the condenser and evaporator sections. The diameter of the pipe, containing these plugs and slug, is d and $L_c$, $L_e$ and $L_{\mathrm{ls}}$ are lengths of the condenser, the evaporator, and the liquid slug, respectively. Heat transfer into the PHP, in the form of sensible and latent heat transfers, causes a pressure difference between the vapor plugs, and this in turn works as a driving force. This makes the liquid slug oscillate in the pipe. For a complete theoretical modeling of PHPs, the following equations have to be solved:

- Conservation of mass for liquid slug and vapor plugs
- Conservation of momentum
- Energy equation for the vapor plugs
- Energy equation for the liquid slug
- Evaporation

- Flow condensation
- Entropy generation equations

### 2.1 Mass conservation equations

This study uses pure water as the working fluid and since the velocity values are not very high, the incompressible assumption can be made with a high accuracy. $L_{\mathrm{ls}}$ changes in each half a cycle of oscillation due to the boiling and condensation processes happening in the pipe. Even though the value of change in this length is negligible, the average change in the mass of neighboring vapor plugs will give the change in the length of the liquid slug:

$$\frac{\mathrm{d}L_{\mathrm{ls}}}{\mathrm{d}t} = \frac{1}{2\rho_l A}\left(\frac{\mathrm{d}m_{\mathrm{vl}}}{\mathrm{d}t} + \frac{\mathrm{d}m_{\mathrm{vr}}}{\mathrm{d}t}\right) \tag{1}$$

The masses of the vapor plugs are changed by the evaporation and condensation phenomena, and the value of this change can be calculated from the mass conservation equation for vapor plugs:

$$\frac{\mathrm{d}m_v}{\mathrm{d}t} = \dot{m}_{\mathrm{boiling}} - \dot{m}_{\mathrm{condensation}} \tag{2}$$

where $\dot{m}_{\mathrm{boiling}}$ and $\dot{m}_{\mathrm{condensation}}$ physically express the rate of vapor mass change due to boiling and condensation that will be calculated as mentioned in the following sections. Sensible heat transfer of the vapor plugs has a small value and the boiling and condensation processes are responsible for the mass transfer into/out of vapor plugs.

### 2.2 Momentum equation of the liquid slug

The above-mentioned incompressible flow assumption will result in the following momentum conservation equation:

$$\rho_l A\frac{\mathrm{d}(L_{\mathrm{ls}}v_{\mathrm{ls}})}{\mathrm{d}t} = [(P_{\mathrm{vl}} - P_{\mathrm{vr}}) - \Delta P_{\mathrm{turn}}]A - \pi\,\mathrm{d}L_{ls}\tau - 2\rho A|x_l - L_e|g \tag{3}$$

This equation shows the force balance exerted on the liquid slug. Left-hand side (LHS) shows the momentum changes of the control volume. The three right-hand side (RHS) terms, from left to right, depict the pressure difference between the two sides of the slug, the momentum reduction due to wall shear stress and the gravitational body force, respectively. Although the value of pressure loss at a single bend is negligible, derivation of exact results is guaranteed by using the following experimental based relation, 3-K model [40]:

$$\Delta P_{\mathrm{turn}} = \frac{K}{d}\rho_l v_{\mathrm{ls}}^2 \tag{4}$$

In which $K$ is the pressure loss coefficient and is calculated from the following equation:

$$K = \frac{K_{\mathrm{Re}}}{\mathrm{Re}} + K_r\left(1 + \frac{K_d}{\left(\frac{d}{0.0254}\right)^{0.3}}\right) \tag{5}$$

Value of the constants for a single 180° turn and ${}^{r_t}/_{d} = 1.25$ are: $K_{\mathrm{Re}} = 1000$, $K_r = 0.1$ and $K_d = 4$ [41].

The shear stress term of the momentum equation is calculated from:

$$\tau = \frac{1}{8} f\rho_l v_{\mathrm{ls}}^2 \tag{6}$$

where $f$ is the friction factor, the value of which for smooth pipes and both laminar and turbulent regimes is given by:

$$f = \begin{cases} \frac{64}{\mathrm{Re}} & \mathrm{Re} \leq 2100 \\ (0.79\ln(\mathrm{Re}) - 1.64)^{-2} & \mathrm{Re} > 2100 \end{cases} \tag{7}$$

2.3 Energy equation of the vapor plugs

Ideal gas assumption is considered for the vapor plugs, so energy equation of the vapor plugs is written by setting $u = c_v T$ and $h = c_p T$:

$$m_v c_v \frac{\mathrm{d}T_v}{\mathrm{d}t} = \left(\dot{m}_{\mathrm{boiling}} - \dot{m}_{\mathrm{condensation},\ v}\right)\mathrm{RT}_v - P_v A \frac{\mathrm{d}x_v}{\mathrm{d}t} \tag{8}$$

The term on LHS depicts the temporal changes of the energy inside the vapor plug. The first and second terms on the RHS demonstrate the energy change resulting from vapor plug mass variations and the work done by or on the vapor plug per unit of time, respectively. It can easily be concluded that $\frac{\mathrm{d}x_{\mathrm{vl}}}{\mathrm{d}t} = \frac{\mathrm{d}x_l}{\mathrm{d}t}$ and $\frac{\mathrm{d}x_{\mathrm{vr}}}{\mathrm{d}t} = -\frac{\mathrm{d}(x_l + L_{\mathrm{ls}})}{\mathrm{d}t}$. The pressure in the vapor plug is expressed by the ideal gas equation of state:

$$P_v V_v = m_v \mathrm{R}\ \mathrm{T}_v \tag{9}$$

2.4 Sensible heat transfer

One-dimensional assumption results in the following energy equation for the single-phase liquid slug, which gives temperature distribution of the liquid slug and sensible heat transfer into and out of the PHP:

$$\frac{1}{\alpha_l}\frac{\mathrm{d}T_l}{\mathrm{d}t} = \frac{\mathrm{d}^2 T_l}{\mathrm{d}x^2} - \frac{H_{l\mathrm{sen}}\pi D}{k_l A}(T_{\mathrm{li}} - T_w) \tag{10}$$

The LHS gives the temporal energy changes inside the liquid slug. The RHS terms indicate the energy distribution due to heat conduction and the energy transfer from/to the lateral surface of the liquid slug to/from the pipe wall. Where $H_{l\mathrm{sen}}$ is the forced convection heat transfer coefficient of the liquid phase. Heat transfer coefficient is corrected by an increment forced convection factor, $E$, to account for the flow boiling in the evaporator section. The value of this factor is calculated by the equation that is defined in the flow boiling section.

Hence:

$$H_{l\mathrm{sen}} = \begin{cases} h_{\mathrm{flow\ boiling}} \\ h_{\mathrm{condensation}} \\ h_{\mathrm{sp}} \end{cases} \tag{11}$$

This equation implies that heat transfer coefficient depends on the flow pattern (two- or single-phase flow) and the flow regime (laminar or turbulent). In the case of a single-phase laminar flow, forced convection heat transfer coefficient ($h_{\mathrm{sp}}$) can be calculated using Shah and London's equation by taking the isothermal wall condition into account and considering thermally developing Hagen–Poiseuille flow: [42]

$$h_{\mathrm{sp}} = \begin{cases} (k_l/d)\left(1.615x^{*\,-\left(\frac{1}{3}\right)} - 0.7\right) & x^* \leq 0.005 \\ (k_l/d)\left(1.615x^{*\,-\left(\frac{1}{3}\right)} - 0.2\right) & 0.005 < x^* < 0.03 \\ (k_l/d)\left(3.657 + \frac{0.0499}{x^*}\right) & x^* > 0.03 \end{cases} \tag{12}$$

The dimensionless $x^*$ is defined as:

$$x^* = \frac{L_e/d}{\mathrm{Re}\cdot\mathrm{Pr}} \tag{13}$$

In the case of single-phase turbulent or transitional flow and with smooth pipe assumption, the Gnielinski's relation is used: [42]

$$h_{\mathrm{sp}} = (k_l/d)\frac{\left(\frac{f}{8}\right)(\mathrm{Re}-1000)\,\mathrm{Pr}}{1+12.7\left(\frac{f}{8}\right)^{0.5}\left(\mathrm{Pr}^{\frac{2}{3}}-1\right)} \quad \mathrm{Re}>2000 \tag{14}$$

In which the value of $f$ is obtained from Eq. (7).

Consequently, having calculated the temperature distribution, the sensible heat flux rate transferred into and out of the PHP for a liquid slug is determined by:

$$q''_{\mathrm{sen,\ in}}(x) = H_{l\mathrm{sen}}(T_l(x,t)-T_w) \quad T_l(x,t)>T_w \tag{15a}$$

$$q''_{\mathrm{sen,\ out}}(x) = H_{l\mathrm{sen}}(T_w-T_l(x,t)) \quad T_l(x,t)<T_w \tag{15b}$$

The total sensible heat transfer rate can be obtained by integrating the heat fluxes over the length of the slug, using following equations:

$$Q_{\mathrm{sen,\ in}}(t) = \int H_{l\mathrm{sen}}\pi\,\mathrm{d}(T_l(x,t)-T_w)\cdot\mathrm{d}x \quad T_l(x,t)>T_w \tag{16}$$

$$Q_{\mathrm{sen,\ out}}(t) = \int H_{l\mathrm{sen}}\pi\,\mathrm{d}(T_w-T_l(x,t))\cdot\mathrm{d}x \quad T_l(x,t)<T_w \tag{17}$$

## 2.5 Flow boiling

The liquid slug oscillates in the pipe and moves into and out of evaporator section. When it enters the evaporator, saturation flow causes boiling and mass gets transferred from the liquid slug to the vapor plug (Fig. 1d). Two dominant boiling mechanisms exist in the microchannels, which are nucleate and convection boiling [43]. Experimental observations show that nucleate boiling mechanism prevails for low Reynolds number of the liquid slug and low quality of vapor in the evaporator [23, 44]. Some correlations for heat transfer in microchannels have been proposed by some researchers [43, 45, 46]. The most known correlations are compared in the study of Cheng [21], in which experimental results are used to establish a database. The results of Cheng show that the correlation of Saitoh et al. [45] gives a better estimation of flow boiling experimental results than other correlations. Therefore, the relation presented by Saitoh et al. is used for the calculation of the boiling heat transfer coefficient in each liquid cell and the two-phase sensible heat transfer increment factor in the evaporator ($E$): [45]

$$h_{\mathrm{flow\ \ boiling}} = \eta h_{\mathrm{boiling}} + E h_{\mathrm{tp}} \tag{18}$$

In the case of laminar or turbulent boiling flow, the following relations, Dittus-Boelter convection heat transfer coefficient ($h_{\mathrm{tp}}$), are used for the calibration: [41]

$$h_{\mathrm{tp}} = \begin{cases} 3.66(k_l/d) & \mathrm{Re}\le 2000 \\ (k_l/d)\left(0.023\mathrm{Re}^{0.8}\,\mathrm{Pr}^{0.4}\right) & \mathrm{Re}>2000 \end{cases} \tag{19}$$

where $E$ is defined by:

$$E = 1+\frac{X_{tt}^{-1.05}}{1+\mathrm{We}_v^{-0.4}} \tag{20}$$

And the Weber number of the vapor phase is:

$$\mathrm{We}_v = \frac{(\rho_l v_{\mathrm{ls}})^2 x_q^2 d}{\sigma \rho_v} \tag{21}$$

According to the definition of the Lockhart–Martinelli Parameter:

$$\begin{cases} X_{tt} = \left(\frac{1-x_q}{x_q}\right)^{0.9} \left(\frac{\rho_v}{\rho_l}\right)^{0.5} \left(\frac{\mu_l}{\mu_v}\right)^{0.1} & \mathrm{Re} > 1000 \\ X_{tt} = \left(\frac{C_l}{C_v}\right)^{0.5} \left(\frac{G_l}{G_v}\right)^{0.5} \mathrm{Re}_v^{-0.4} \left(\frac{\rho_v}{\rho_l}\right)^{0.5} \left(\frac{\mu_l}{\mu_v}\right)^{0.1} & \mathrm{Re} < 1000 \end{cases} \tag{22}$$

The local vapor quality at each area section of the evaporator is denoted by $x_q$, which is defined as the rate of vapor mass flow into an arbitrary area section of the evaporator (mass rate of boiling) divided by the local flow rate of the liquid slug going in/out of the area section. So, in the boiling section of the liquid slug, $x_q(t)$ can be found by:

$$x_q(t) = \frac{\dot{m}_{\mathrm{boiling}}(t)}{\dot{m}_l(t) + \dot{m}_{\mathrm{boiling}}(t)} \approx \frac{\dot{m}_{\mathrm{boiling}}(t)}{\dot{m}_l(t)} \tag{23}$$

$h_{\mathrm{boiling}}$ is the boiling heat transfer coefficient and is given by Saitoh et al.:

$$h_{\mathrm{boiling}}(x,t) = 207 \frac{k_l}{d_b(t)} \left(\frac{q''(x,t) d_b(t)}{k_l T_l(x,t)}\right)^{0.745} \left(\frac{\rho_v}{\rho_l}\right)^{0.581} \mathrm{Pr}^{0.533} \tag{24}$$

where $d_b(t)$ is:

$$d_b(t) = 0.51 \left(\frac{2\sigma}{g(\rho_l - \rho_v(t))}\right)^{0.5} \tag{25}$$

$\rho_v(t)$ in Eq. (25) is calculated using the ideal gas assumption of the vapor phase. $q''(x,t)$ is the sensible heat flux rate in an arbitrary location of the liquid phase in the evaporator, and it is obtained using Eq. (15a).

The boiling heat transfer corrector, $\eta$, in Eq. (18) is:

$$\eta(t) = \frac{1}{1 + 0.4\left(10^{-4} \times \mathrm{Re} \cdot E^{1.25}\right)^{1.4}} \tag{26}$$

As a result, the boiling process share of the heat transfer rate into the PHP can be obtained by:

$$\dot{\mathrm{Q}}_{\mathrm{boiling}}(t) = \int \eta(t) h_{\mathrm{boiling}}(x,t) \pi d (T_w - T_l(x,t)) \mathrm{d}x \quad \text{if} \quad T_w > T_l(x,t) \tag{27}$$

And finally, the mass that is transferred into the vapor plugs per unit of time is calculated from:

$$\dot{m}_{\mathrm{boiling}}(t) = \frac{\dot{Q}_{\mathrm{boiling}}(t)}{h_{fg}} \tag{28}$$

### 2.6 Flow condensation

Condensation in vapor plug that enters the condenser, occurs as a result of a low wall temperature. Condensation is significantly affected by the flow pattern [47]. The temperature of the liquid layer adjacent to the condenser wall is lower and as a result, it has a higher viscosity, which causes the formation of a thin liquid film on the cooling wall as shown in Fig. 1c. So as presented in the experimental studies of Tong et al. and Khandekar et al. [23, 48], annular flow assumption can be made for this region. Many researchers [49–52] have

presented correlations for the evaluation of condensation in mini/micro-channels. A database of empirical results has been collected by Ribatski et al. [47] and the suggested correlations have been compared. This comparison shows that the relation proposed by Cavallini et al. [50] gives the best predictions. So, the authors recommended this correlation to be used in the design of heat exchangers. Based on these findings, the method of Cavallini et al. is used in this study to calculate local flow condensation heat transfer coefficient:

$$h_{\text{condensation}}(x,t) = H_{l\text{sen}}(x)\left[1+1.128x_q(x,t)^{0.817}\left(\frac{\rho_l}{\rho_{v(t)}}\right)^{0.3685}\left(\frac{\mu_l}{\mu_v}\right)^{0.2363}\left(1-\frac{\mu_v}{\mu_l}\right)^{2.144}\text{Pr}^{-0.1}\right] \tag{29}$$

This equation represents the heat transfer coefficient in the condenser section, which depends on thermo-physical characteristics of the vapor and the liquid phases. Furthermore, this coefficient is a function of the quality of the vapor, $x_q(x,t)$, in an arbitrary area section of the condenser. A thin liquid film forms in the condenser section and this leads to annular flow in the region (see Fig. 1c). Thus, the vapor quality can be evaluated using the liquid film thickness, $\delta_{\text{film}}$:

$$x_q(x,t) = \frac{m_v(x,t)}{m_{\text{tot}}} = \frac{V_v\rho_v}{V_v\rho_v + V_l\rho_l} = \frac{\left(\frac{d}{2}-\delta_{\text{film}}(t)\right)^2\rho_v}{\left(\frac{d}{2}-\delta_{\text{film}}(t)\right)^2\rho_v + \left[\left(\frac{d}{2}\right)^2-\left(\frac{d}{2}-\delta_{\text{film}}(t)\right)^2\right]\rho_l} \tag{30}$$

For determination of liquid film thickness, Han et al. [53] presented an empirical correlation with an accuracy of 15%, as follows:

$$\frac{\delta_{\text{film}}(t)}{d} = \begin{cases} \dfrac{0.670\text{Ca}_{(t)}^{\frac{2}{3}}}{1+3.13\text{Ca}_{(t)}^{\frac{2}{3}}+0.504\text{Ca}_{(t)}^{0.672}\text{Re}_{(t)}^{0.589}-0.352\text{We}_{(t)}^{0.629}} & \text{Re}(t)\le 2000 \\ \dfrac{106.0\left(\frac{\mu^2}{\rho\sigma d}\right)^{\frac{2}{3}}}{1+497.0\left(\frac{\mu^2}{\rho\sigma d}\right)^{\frac{2}{3}}+7330\left(\frac{\mu^2}{\rho\sigma d}\right)^{0.672}-5000\left(\frac{\mu^2}{\rho\sigma d}\right)^{0.629}} & \text{Re}(t)>2000 \end{cases} \tag{31}$$

As can be seen in Eq. (31), $\delta_{\text{film}}$ only depends on time; i.e., uniform thickness through the condenser length has been considered for the liquid film in this study. Except the liquid–vapor interface, this assumption is physically acceptable in annular flow region.

Assuming homogenous vapor plugs and uniform quantities, the average condensation heat transfer coefficient can be calculated by integration of the local condensation heat transfer along the condenser length:

$$h_{\text{condensation}}(t) = h_{tp}\left[1+1.128x_q(t)^{0.817}\left(\frac{\rho_l}{\rho_v}\right)^{0.3685}\left(\frac{\mu_l}{\mu_v}\right)^{0.2363}\left(1-\frac{\mu_v}{\mu_l}\right)^{2.144}\text{Pr}^{-0.1}\right] \tag{32}$$

$h_{\text{tp}}$ is the sensible heat transfer, the value of which can be evaluated from Eq. (19).

As temporal condensation heat transfer coefficient and temperature difference between the vapor plug and the wall is known, the latent heat transferred out of the PHP due to the flow condensation can be calculated by:

$$\dot{Q}_{\text{condensation}}(t) = h_{\text{condensation}}(t)\pi d|x_l(t)-L_e|(T_v(t)-T_w) \quad \text{if } T_w < T_v(t) \tag{33}$$

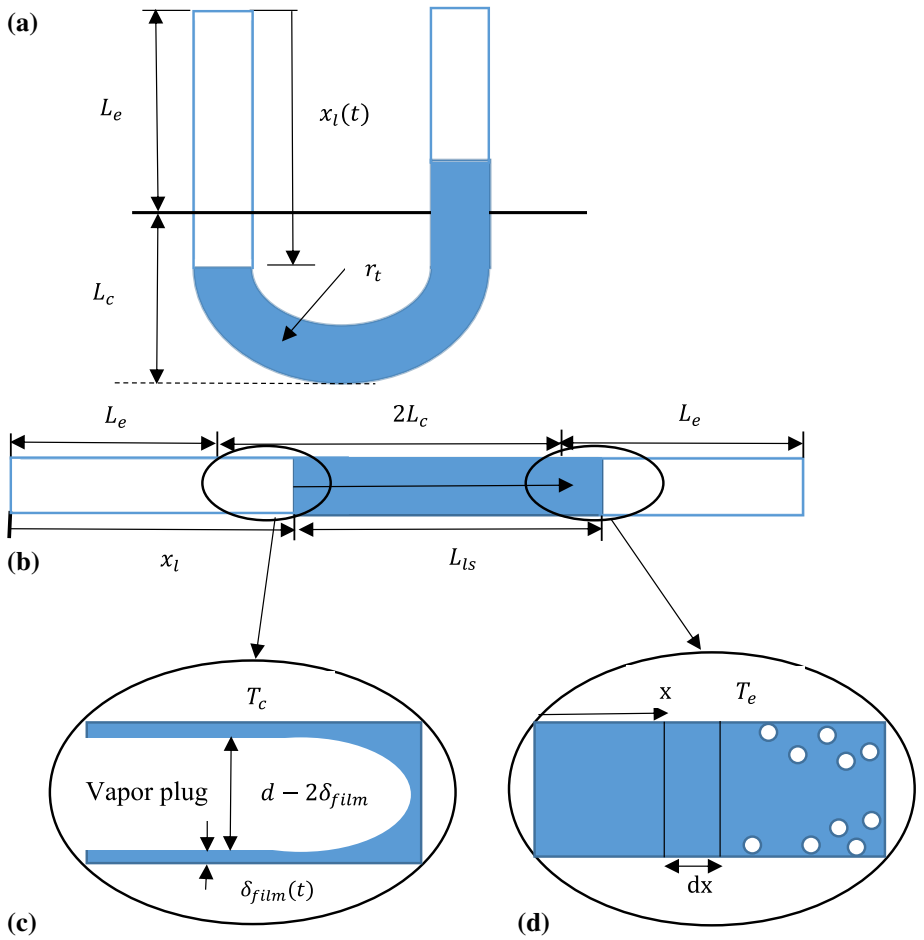


**Fig. 1** Schematic of a single-turn pulsating heat pipe, **a** U-turn, **b** Linear pipe configuration **c** Condenser section **d** Evaporator section

And finally, the mass transfer out of the vapor plugs is as follows:

$$\dot{m}_{\text{condensation}} = \frac{\dot{Q}_{\text{condensation}}(t)}{h_{fg}} \tag{34}$$

## 2.7 Entropy generation

For entropy generation analysis, the total entropy generation is sum of the viscous flow-induced entropy generation and the entropy generation resulting from heat transfer:

$$\dot{S}_{\text{gen, }T}(t) = \dot{S}_{\text{gen, }F}(t) + \dot{S}_{\text{gen, th}}(t) \tag{35}$$

The entropy generation resulting from heat transfer consists of latent heat- and sensible heat- induced entropy generations, i.e.:

$$\dot{S}_{\text{gen, th}}(t) = \dot{S}_{\text{gen, late}}(t) + \dot{S}_{\text{gen, sen}}(t) \tag{36}$$

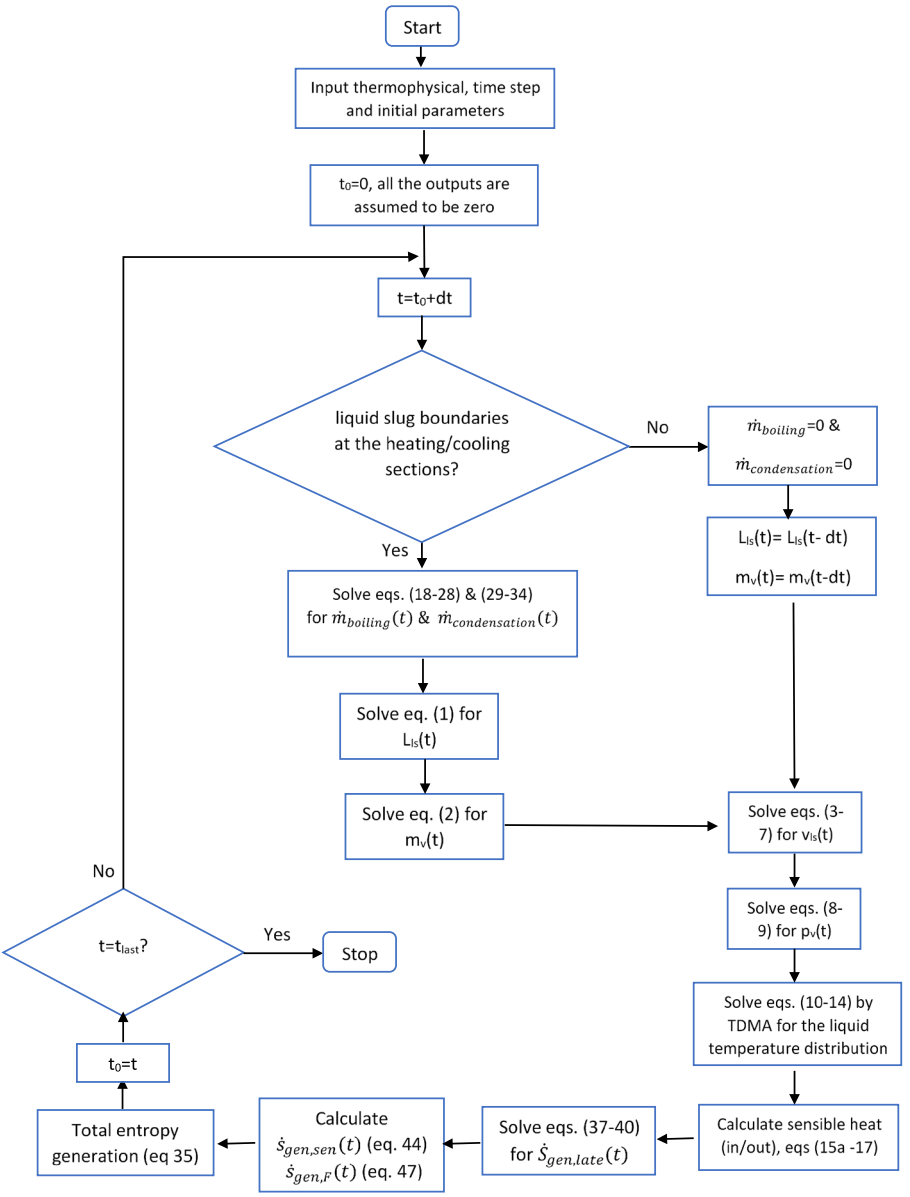


**Fig. 2** Flow chart of the solution

The entropy generation resulting from latent heat transfer is:

$$\dot{S}_{\text{gen, late}}(t) = \frac{\dot{Q}_{\text{boiling}}(t)}{T_e} - \frac{\dot{Q}_{\text{condensation}}(t)}{T_c} + \frac{\Delta S_v}{\Delta t} \tag{37}$$

The first term accounts for the changes in entropy due to the latent heat transfer in the evaporator section, in which heat is transferred to the liquid slug. The second term represents the changes in entropy in the condenser section that are due to the latent heat. The third term,

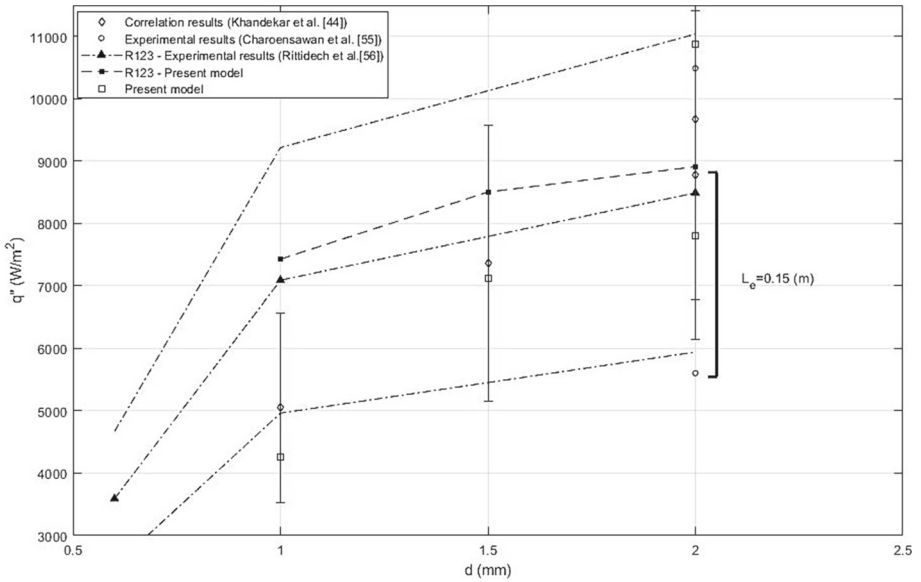


**Fig. 3** Comparison of the heat flux calculated in the present model with experimental results of Charoensawan et al. [55], Rittidech et al. [56] and Khandekar et al. [44] correlation data

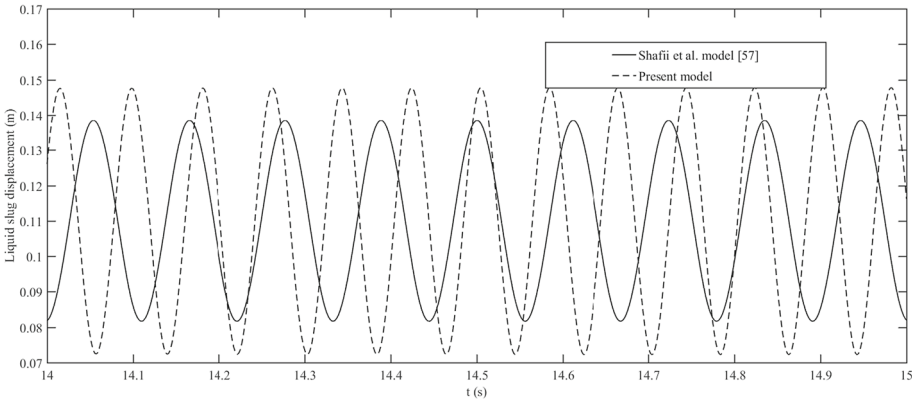


**Fig. 4** Comparison of the liquid slug displacement derived with the present model with those of Shafii et al. [57]

which is entropy generation caused by the mass changes in vapor plug, is determined by the following equation:

$$\Delta S_v = \frac{\mathrm{d}}{\mathrm{d}t}(ms)\Delta t = \left[\frac{\mathrm{d}m}{\mathrm{d}t}s_v + m\frac{\mathrm{d}s}{\mathrm{d}t}\right]\Delta t \tag{38}$$

The rate of the mass change due to condensation and evaporation, $\frac{dm}{\mathrm{d}t}$, is detected by Eq. (2). The rate of the entropy generation changes is calculated by the following equation. The ideal gas assumption has been applied to the vapor plug.

$$\left.\frac{\mathrm{d}s}{\mathrm{d}t}\right|_v = c_p\frac{\mathrm{d}T}{T} - R\frac{\mathrm{d}P}{P} \tag{39}$$

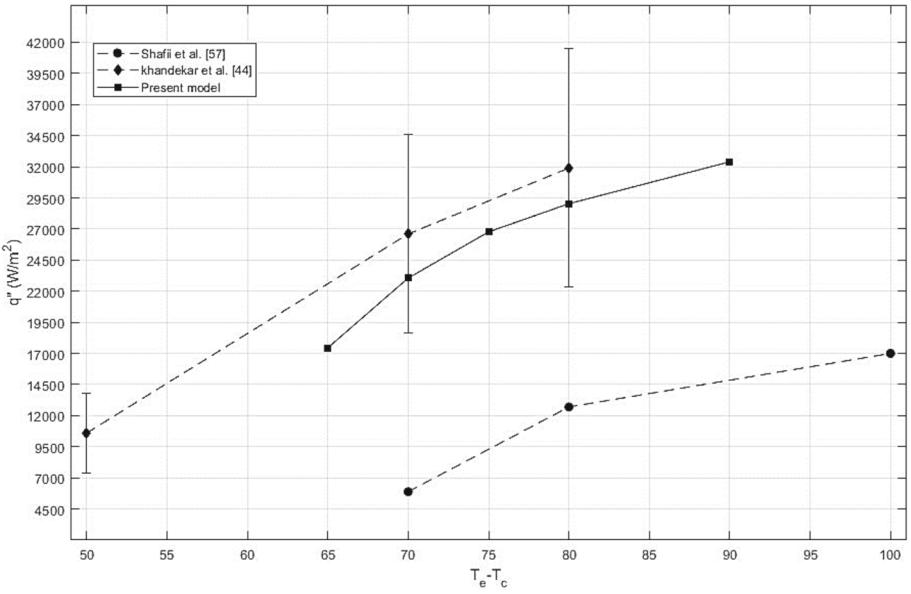


**Fig. 5** Comparison of the heat flux derived for various temperature differences in the present model with those of Shafii et al. [57] and Khandekar et al. [44]

The entropy generation resulting from mass changes of the vapor is calculated by:

$$\Delta S_v(t) = \left(\dot{m}_{\text{boiling}}(t) - \dot{m}_{\text{condensation}}(t)\right) s_v(t)\Delta t + m_v(t)\left[c_p \ln \frac{T(t)}{T(t-\Delta t)} - R \ln \frac{P(t)}{P(t-\Delta t)}\right]\Delta t \tag{40}$$

The entropy generation resulting from fluid flow and the sensible heat transfer can be evaluated by the following equation [54]:

$$\dot{S}'_{\text{gen}} = \frac{q'\Delta T}{T^2} + \frac{\dot{m}}{\rho T}\left(-\frac{\mathrm{d}P}{\mathrm{d}x}\right) \tag{41}$$

The heat flux is calculated as:

$$q'(t) = \pi \mathrm{d}\Delta T(t) h_{\text{sp}}(t)\mathrm{d}x \tag{42}$$

Besides, the share of sensible heat transfer in entropy generation per length unit is determined from:

$$\dot{S}'_{\text{gen}}(t) = \pi \mathrm{d}\left(\frac{T_w - T_L(x,t)}{T_L(x,t)}\right)^2 h_{\text{sp}}\mathrm{d}x \tag{43}$$

$T_L(x,t)$, the temperature distribution of the liquid slug, is a function of the time and location. The following equation can be used for calculation of the entropy generation caused by the sensible heat transfer:

$$\dot{S}_{\text{gen, sen}}(t) = \int_0^{L_l} \pi \mathrm{d}\left(\frac{T_w - T_L(x,t)}{T_L(x\cdot t)}\right)^2 h_{\text{sp}}\mathrm{d}x \tag{44}$$

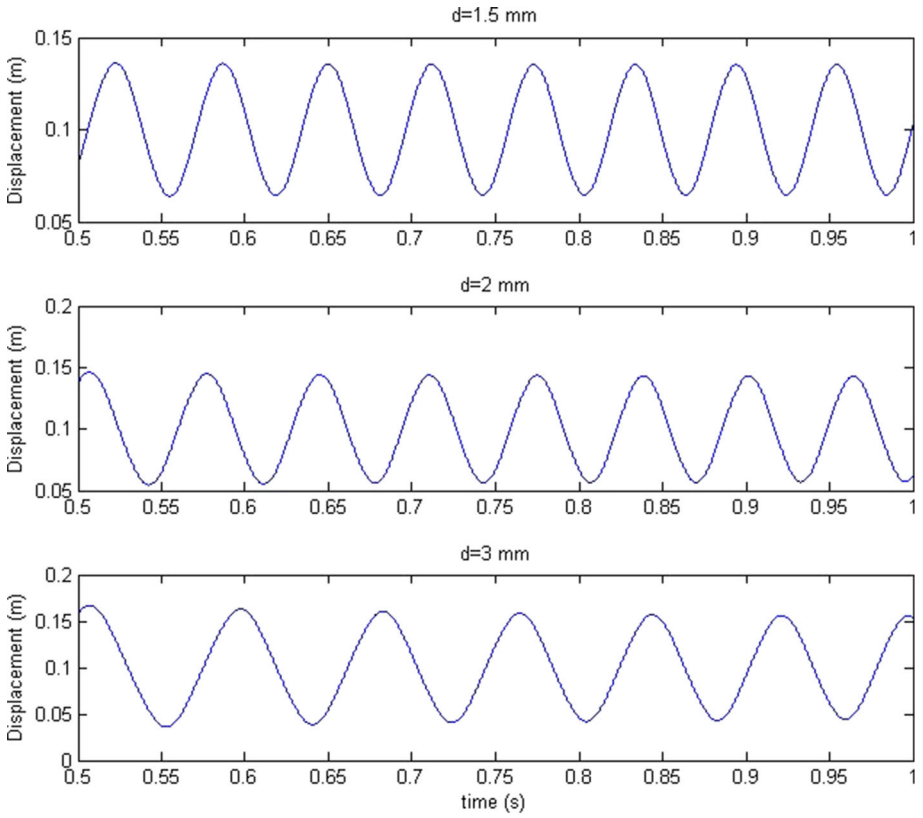


**Fig. 6** Displacement of the liquid slug for different pipe diameters

Viscous flow-induced entropy generation is:

$$\dot{S}_{\text{gen, }F}(t) = \int_0^{L_l} \frac{\dot{m}}{\rho T_L(x,t)} \frac{2C_{\text{li}}}{d} \rho V^2 \mathrm{d}x \tag{45}$$

The Darcy–Weisbach friction coefficient is $f = 4\ C_{\text{li}}$. The following equation is defined to convert the pressure drop in the bend of the pipe (i.e., local drops):

$$L_{\text{eq}} = \frac{d}{2C_{\text{li}}} \Delta P_b \frac{1}{\rho v^2} \tag{46}$$

Thus, the entropy generation caused by the viscous flow can be calculated by:

$$\dot{S}_{\text{gen, }F}(t) = \pi \mathrm{d} f \frac{\rho v^3}{2} \int_0^{L_l + L_{\text{eq}}} \frac{1}{T_L(x,t)} \mathrm{d}x \tag{47}$$

## 2.8 Algorithm of numerical solution

The mass and momentum conservation equations for the liquid slug are solved using an explicit finite difference scheme for determination of the new values of the parameters at the next time step from the old values. Furthermore, the mass and energy equations of the

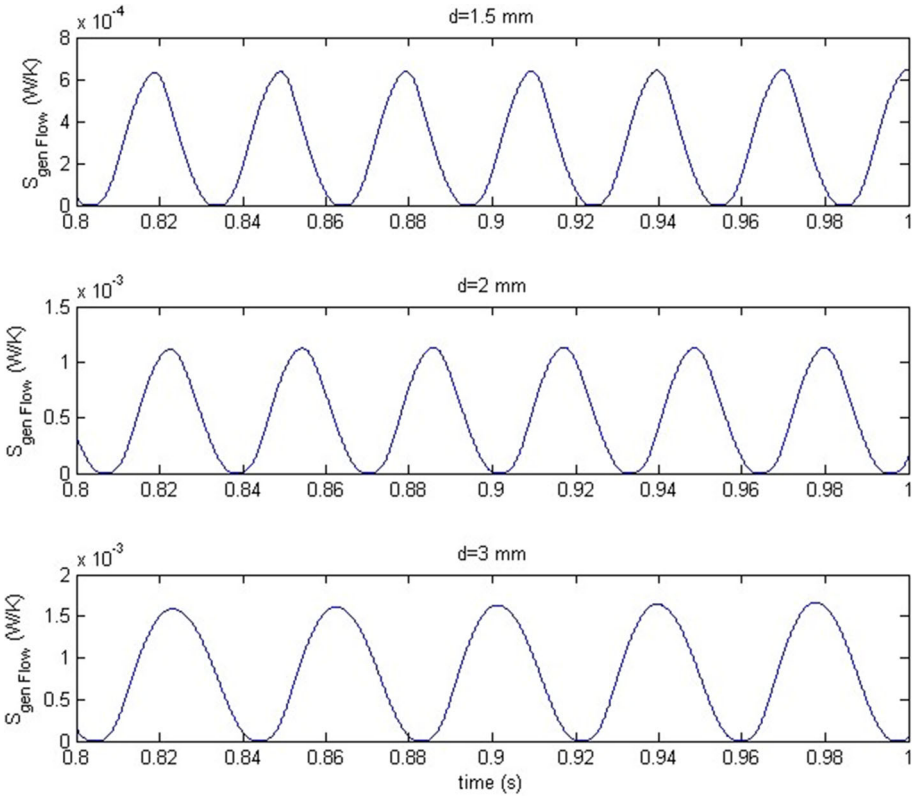


**Fig. 7** Entropy generation resulting from the viscous flow of the liquid slug

vapor plugs are also solved by explicit scheme. The following are the discretized form of the momentum and the energy equations of the liquid slug and the vapor plugs, respectively:

$$(L_{\mathrm{ls}} v_{\mathrm{ls}})^{n+1} = \frac{1}{\rho_l A}([(P_{\mathrm{vl}} - P_{\mathrm{vr}}) - \Delta P_{\mathrm{bend}}]A - \pi d L_{ls}\tau - 2\rho A|x_l - L_e|g)^n \cdot \Delta t + (L_{\mathrm{ls}} v_{\mathrm{ls}})^n \tag{48}$$

$$T_v^{n+1} = \left(\frac{1}{m_v c_v}\left(\dot{m}_{\mathrm{boiling}\cdot v} - \dot{m}_{\mathrm{condensation},\, v}\right)\mathrm{RT}_v\right)^n - \frac{1}{m_v^n c_v}(P_v A)^n\left(x_l^{n+1} - x_l^n\right) \tag{49}$$

The temperature distribution and the sensible heat transfer equations are solved using TDMA (Tri-diagonal Matrix Method) with a time step value of $10^{-4}$ which makes the solutions independent of the time step. The entropy generation equations are solved using the time and space dependent temperature distribution. The solution flow chart of the aforementioned equations is depicted in Fig. 2. The mesh structure is non-uniform and consists of 1200 nodes. 400 cells belong to each end of the slug, with the length of 0.04 m, and 400 cells belong to the rest of the slug which has an insignificant role in the heat transfer mechanism.

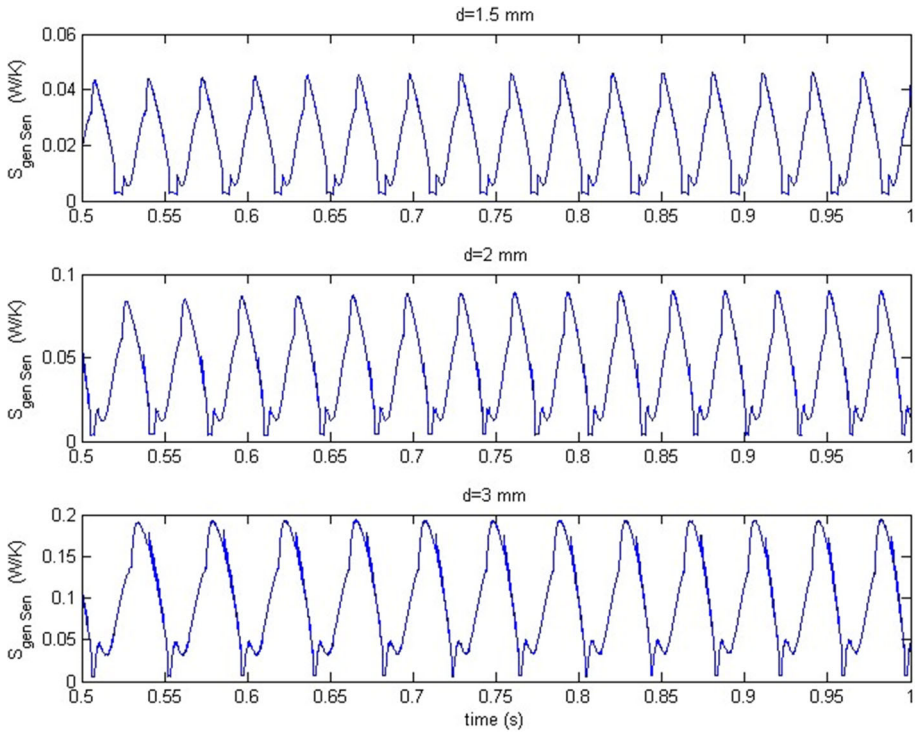


**Fig. 8** Entropy generation caused by the sensible heat transfer into and out of the liquid slug

## 3 Results

The working fluid in this study is assumed to be water and its characteristics are used in the code that has been developed to solve the above-mentioned equations. In order to show the correctness and the accuracy of the presented results, the numerical solution is validated using the empirical results of Charoensawan et al. [55] and correlation of Khandekar et al. [44]. In the experimental heat transfer study of Charoensawan et al., a multi-turn PHP has been used. The results of this study have been presented based on the diameter of the pipe, number of the turns and the length of the evaporator. On the other hand, in the empirical and numerical studies (of Zhang et al. [15, 16], Tong et al. [23], Khandekar et al. [39]) it has been shown that for a small number of turns, the heat transfer is not affected by the turns. Based on these studies and conclusions, the results of works with a small number of turns are used for validation of the heat transfer results of the single-turn PHP in this paper. Two other conditions exist in the work of Charoensawan et al. First the temperature of the condenser is set to 20 °C and the evaporator to 80°, which means that isothermal wall conditions is applied as the boundary condition. Second, the length of the evaporator and condenser sections are set to be equal, which in turn results in 50% filling ratio for the pipe. By correlating the empirical data of Charoensawan et al., Khandekar et al. presented a correlation that has an overall drift within ±30% limit, which is:

$$q'' = 0.54\mathrm{Ka}^{0.47}\,\mathrm{Pr}^{0.27}\,\mathrm{Ja}^{1.43}N_t^{-0.27} \tag{50}$$

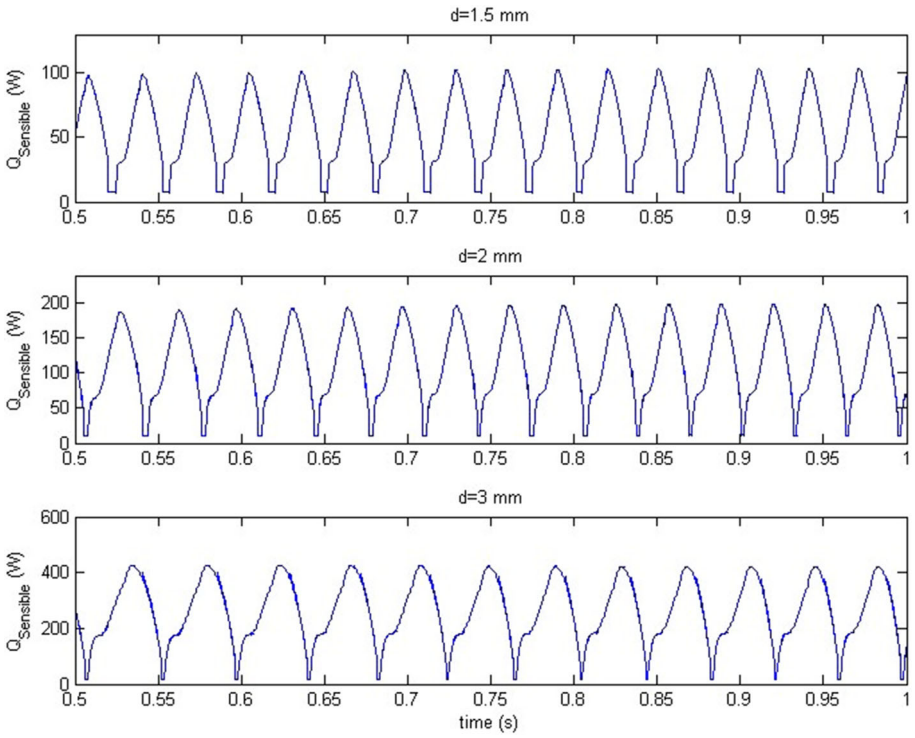


**Fig. 9** Sensible heat transfer of the liquid slug

As mentioned above, heat transfer values have been used for validation, and Fig. 3 depicts the comparison of current work with empirical results of Charoensawan et al. [55], Rittidech et al. [56] and the correlation of Khandekar et al. [44]. This figure suggests that the current model is able to closely simulate the phenomena with a good degree of accuracy. In all presented cases, $\Delta T = \mathrm{T}_e - \mathrm{T}_c = 60$ °C, $L_c = L_e = L_{\mathrm{ls}}$ and $L_e$ is 0.1 m, except a single case, for which $L_e = 0.15$ m. Dashed lines in this figure are the data for R123. This working fluid has only been used for validation of this model using the empirical data from Rittidech et al. and in all other cases the working fluid of the PHP is water. For R123 the length of the evaporator section is set to 50 mm in order to simulate the conditions used for the corresponding experimental data. The results presented here show that increase in the size of the evaporator section, reduces heat transfer capacity of the pipe and this conclusion is in agreement with other experimental studies, e.g., Rittidech [56].

The second part of the validation of the current model is based on the displacement of the liquid slug. Figure 4 Depicts this value at different times and presents a comparison of the results with those of Shafii et al. [57]. The data presented in this figure are driven by following considerations:

$\Delta T = T_e - T_c = 100$ °C, $Le = 0.1$ m, $2Lc = 0.37$ m, $L_{\mathrm{ls}} = 0.35$ m (results in 61.4% of filling ratio) and $d = 1.5$ mm.

As can be seen in this figure, there is a small difference in frequency and amplitude of the oscillations between the presented results and the values corresponding to the current study are slightly higher than the results of Shafii et al. The source of this difference can be the assumptions made in the study of Shafii et al. These assumptions include the constant

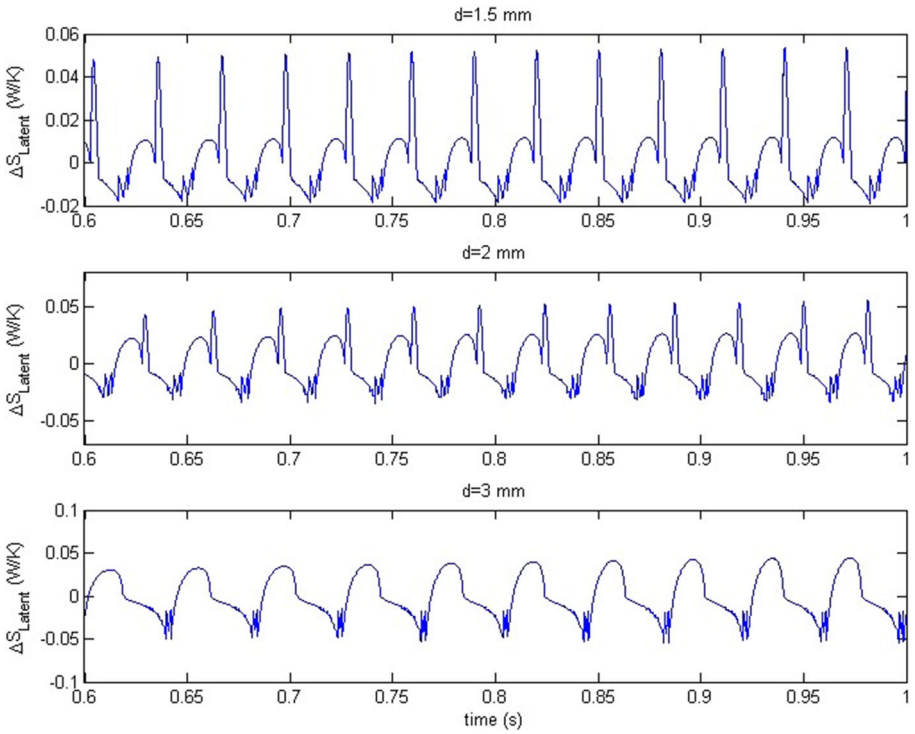


**Fig. 10** Entropy generation resulting from the latent heat transfer of the phase change

evaporative and condensation coefficients and neglecting flow boiling heat transfer coefficient. When two-phase heat transfer coefficients increase, the amount of mass transfer into the vapor plugs increases and this, in turn, increases the transmission speed between condenser and evaporator sections. Increased value of the amplitude and frequency values play an important role in the sensible heat transfer and performance of PHPs.

The results from Shafii et al. [57] and Khandekar et al. [44] are compared to that of the present model in Fig. 5. This figure illustrates the values of heat flux for various temperature differences at condenser and evaporator. The heat flux values derived using current model are close to the exact values that have been presented by Khandekar et al. [44].

The displacement of the liquid slug is depicted in Fig. 6 and a slight decrease in the frequency as a result of diameter increase can easily be seen. The amplitude of the oscillations on the other hand increases by diameter. The values presented in Fig. 6 are in complete agreement with all previous studies that have been conducted on the diameter effect in pulsating heat pipes.

Figure 7 illustrates the entropy generation resulting from the viscous flow of the liquid slug in the pipe. This process generates entropy as a result of the irreversibilities associated with friction and viscosity. The properties of the pipe are set as: $\Delta T = T_e - T_c = 80$ °C, $Le = L_c = 0.1$ m, $L_{ls} = 0.2$ m (results in 50% of filling ratio). These values remain unchanged in the rest of the study. However, the diameter of the PHP is changed to assess its contribution in entropy generation and heat pipe performance. It can clearly be seen from the figure that the amplitude of the oscillations increases dramatically as the diameter increases. This increase amounts to about 50% of its value. Moreover, the frequency of oscillations decreases

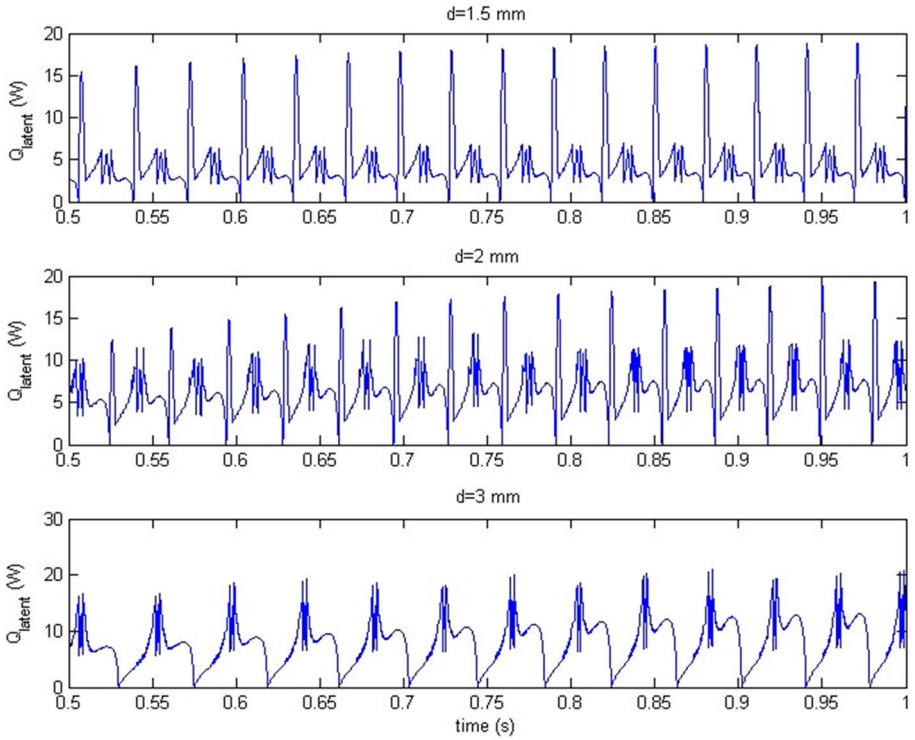


**Fig. 11** Latent heat transfer of phase change

slightly as the diameter size increase from 1.5 to 3 mm. Increase in diameter decreases the value of the retarding force that is applied to the liquid slug and this in turn increases the displacement capability of the slug and results in increased amplitude and decreased frequency; in agreement with other studies. These effects directly influence the entropy generation that results from the flow.

Figure 8 shows the entropy generation associated with sensible heat transfer into and out of the liquid slug. As depicted in this figure, the value of entropy generation increases dramatically as the value of the diameter increases. Increase in diameter of the pipe rises the amount of heat transfer of the liquid slug. Thus, the improved heat transfer causes an increase in the generated entropy. Contrary to the amplitude of oscillations, which increases, the frequency decreases slightly. This drop in frequency is the result of frequency decrease of the displacement of the liquid slug.

Figure 9 presents the value of heat transfer of the liquid slug, which is sum of the heat lost in the condenser region and gained in the evaporator section. This figure shows that the heat transfer value or the amplitude of oscillations of heat transfer largely grows as the diameter of the pulsating heat pipe increases. Thus, it justifies the dramatic entropy generation increase of Fig. 8 and is in complete agreement with it. The insignificant decrease of frequency also obeys the pattern of entropy generation and liquid displacement.

Figure 10 demonstrates the entropy generation resulting from the latent heat transfer of the phase change. Increase in the average value of the entropy generation by an increase of the diameter is evident in this figure. The reason for this change is clearly seen in Fig. 11,

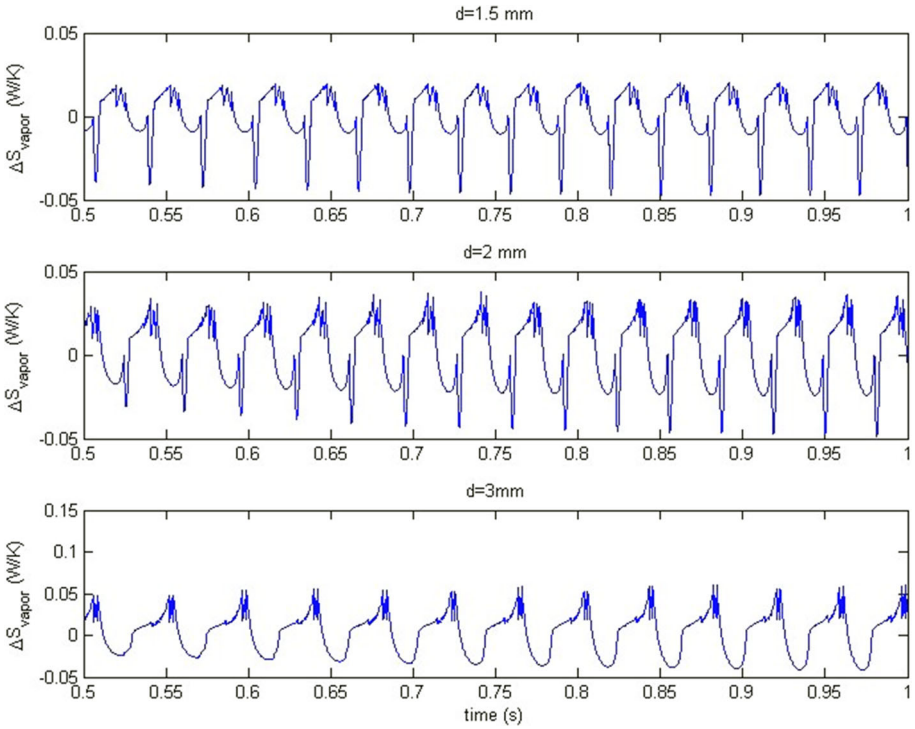


**Fig. 12** Entropy changes in the vapor plugs for different pipe diameters

which depicts the latent heat transfer of the phase change. Increase in latent heat produces an increase in the entropy generation caused by latent heat transfer. As depicted in the diagrams above, amplitude increase and frequency decrease are two effects that occur with enlargement of the pipe diameter.

Figure 12 illustrates changes in the entropy in the vapor plugs of the PHP. These values are sum of the entropy change in two plugs by which the liquid slug has been surrounded. Amplitude and frequency of the oscillations in these vapor plugs obey the above pattern, in which the amplitude increases and the frequency decreases slightly.

Figure 13 shows the total entropy generation in the PHP system, which includes sensible and latent heat transfers and flow-induced entropy generation. This system consists of a liquid slug and two vapor plugs that surround this slug. It is clearly visible in this figure that total entropy generation grows significantly as the diameter of the pipe increases. This dramatic rise can be defined as performance increase of the PHP which has an increasing effect on the entropy generation. Besides the amplitude boost, a small decrease can be detected in the frequency of oscillations, which can be justified by the change in the displacement frequency.

Bejan number, which lies in the limit of $0 \leq \mathrm{Bej} \leq 1$, represents the ratio of viscous-flow-induced entropy generation and heat transfer induced entropy generation. So that when $\mathrm{Bej} > 0.5$, the entropy generation resulting from heat transfer dominates; and when $\mathrm{Bej} < 0.5$, entropy generation due to viscous flow is the dominant entropy generation mechanism. Figure 14 presents Bej number values for different pipe diameters. The increase of Bejan number in diameter $d = 3$ mm is clearly seen in this figure Heat transfer share in entropy generation is the greatest at this diameter and this is the optimum aim in PHP design.

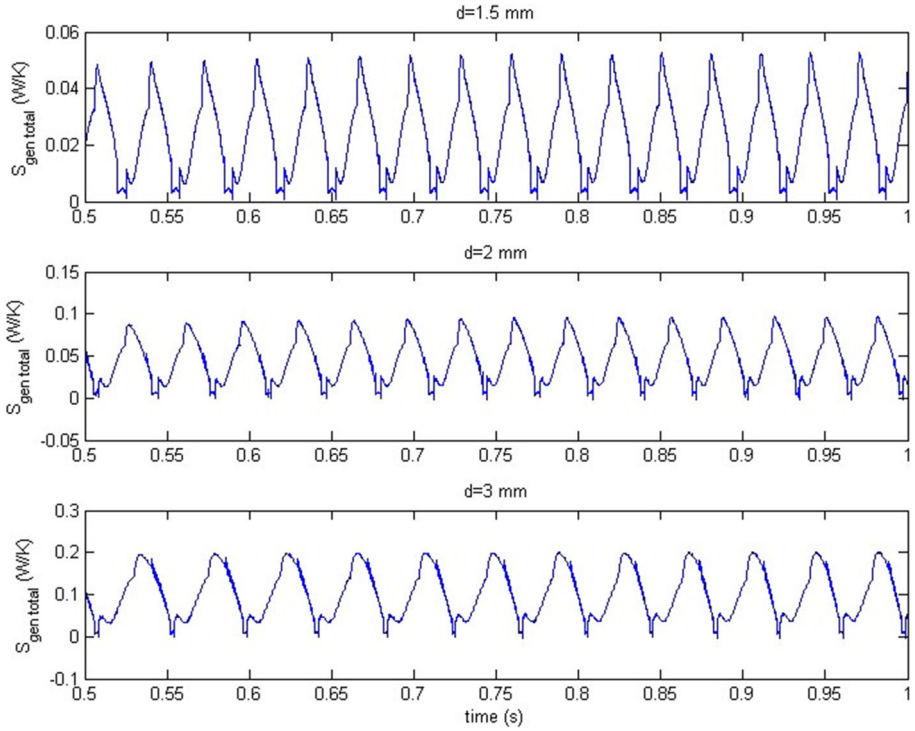


**Fig. 13** Total entropy generation of the PHP for different pipe diameters

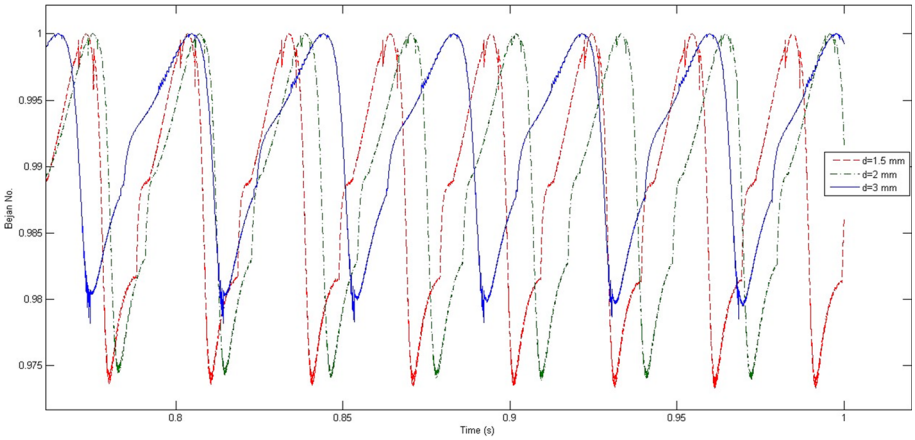


**Fig. 14** Bejan number for different pipe diameters

## 4 Conclusion

A pulsating heat pipe with a single liquid slug, surrounded by two vapor plugs has been studied in this work. Working fluid in this model is pure water and it is unchanged through the whole study. Most of the previous numerical studies in this field are presented for con-

stant heat flux case and boiling and condensation mechanisms are neglected. On the other hand, the models available for constant temperature boundary condition and thin-film boiling require substantial increase in the accuracy. The present study fills this gap for constant temperature boundary conditions in evaporator and condenser sections utilizing the best predicting correlations. In this work, except energy equation of the liquid slug, all fundamental equations are solved by an explicit method. Along the best correlations used for the calculation of boiling and condensation, entropy generations caused by different factors have also been computed. The entropy generation method that has attracted many researchers recently, is a key factor in optimization of different devices, especially heat exchangers. The results reveal an inverse relationship between the size of the heating section and the heat transfer performance, which is confirmed by the experimental data [56]. The results are presented for three different diameter values of the pipe. These are in agreement with all other studies and show that increase in diameter causes an rise in the amplitude and a slight decrease in the frequency of the oscillations [15]. The augmentation of the amplitude is due to lower retarding force in the larger diameters. Moreover, the pipe diameter increase enhances the heat transfer, which is consistent with the previous works [55–57]. The results of entropy generation indicate that the entropy generation in the pulsating flows grows with diameter, because of the larger gradients of the temperature and velocity. This phenomenon has also been reported in the previous studies [58–61]. A decrease in frequency of oscillations is evident in all above-mentioned results, and it is due to the change in displacement pattern, which in turn is a result of the lower retarding force applied to the slug in larger diameters.

Bejan number has also been evaluated and it depicts that the increase of the diameter to 3 mm, has caused the heat transfer share in entropy generation to be the highest at this diameter. Generally, the dominant share in entropy generation is due to the heat transfer in PHPs, bringing Bejan number close to unity, which is consistent with the findings of previous studies on pulsating flow in pipe [61]. Hence, the heat transfer diagrams are in agreement with the entropy changes and show the same behavior.

## References


1. L. Vasiliev et al., Loop heat pipe for cooling of high-power electronic components. Int. J. Heat Mass Transf. **52**(1), 301–308 (2009). https://doi.org/10.1016/j.ijheatmasstransfer.2008.06.016
2. Y.-C. Weng, H.-P. Cho, C.-C. Chang, S.-L. Chen, Heat pipe with PCM for electronic cooling. Appl. Energy **88**(5), 1825–1833 (2011). https://doi.org/10.1016/j.apenergy.2010.12.004
3. P. Warrier, A. Sathyanarayana, D.V. Patil, S. France, Y. Joshi, A.S. Teja, Novel heat transfer fluids for direct immersion phase change cooling of electronic systems. Int. J. Heat Mass Transf. **55**(13), 3379–3385 (2012). https://doi.org/10.1016/j.ijheatmasstransfer.2012.02.063
4. A. Renfer et al., Microvortex-enhanced heat transfer in 3D-integrated liquid cooling of electronic chip stacks. Int. J. Heat Mass Transf. **65**, 33–43 (2013). https://doi.org/10.1016/j.ijheatmasstransfer.2013.05.066
5. Y. Cheng, J. Xu, Y. Sui, Numerical study on drag reduction and heat transfer enhancement in microchannels with superhydrophobic surfaces for electronic cooling. Appl. Therm. Eng. **88**, 71–81 (2015). https://doi.org/10.1016/j.applthermaleng.2014.10.058
6. M. Adamski, *Dynamical Characteristics of Exchangers with Phase Change* (Bialystok, Poland, 2008).
7. M. Adamski, Heat transfer correlations and NTU number for the longitudinal flow spiral recuperators. Appl. Therm. Eng. **29**(2), 591–596 (2009). https://doi.org/10.1016/j.applthermaleng.2008.03.029
8. Q. Long, X.Y. Xu, K.V. Ramnarine, P. Hoskins, Numerical investigation of physiologically realistic pulsatile flow through arterial stenosis. J. Biomech. **34**(10), 1229–1242 (2001). https://doi.org/10.1016/S0021-9290(01)00100-2
9. R.A. El-Nabulsi, Dynamics of pulsatile flows through microtubes from nonlocality. Mech. Res. Commun. **86**, 18–26 (2017). https://doi.org/10.1016/j.mechrescom.2017.10.005

10. I. Marshall, S. Zhao, P. Papathanasopoulou, P. Hoskins, X.Y. Xu, MRI and CFD studies of pulsatile flow in healthy and stenosed carotid bifurcation models. J. Biomech. **37**(5), 679–687 (2004). https://doi.org/10.1016/j.jbiomech.2003.09.032
11. D.S. Sankar, K. Hemalatha, Pulsatile flow of Herschel–Bulkley fluid through stenosed arteries—a mathematical model. Int. J. Non-Linear Mech. **41**(8), 979–990 (2006). https://doi.org/10.1016/j.ijnonlinmec.2006.02.007
12. R.A. El-Nabulsi, Nonlocal-in-time kinetic energy in nonconservative fractional systems, disordered dynamics, jerk and snap and oscillatory motions in the rotating fluid tube. Int. J. Non-Linear Mech. **93**, 65–81 (2017). https://doi.org/10.1016/j.ijnonlinmec.2017.04.010
13. X. Han, X. Wang, H. Zheng, X. Xu, G. Chen, Review of the development of pulsating heat pipe for heat dissipation. Renew. Sustain. Energy Rev. **59**, 692–709 (2016). https://doi.org/10.1016/j.rser.2015.12.350
14. D. Bastakoti, H. Zhang, D. Li, W. Cai, F. Li, An overview on the developing trend of pulsating heat pipe and its performance. Appl. Therm. Eng. **141**, 305–332 (2018). https://doi.org/10.1016/j.applthermaleng.2018.05.121
15. Y. Zhang, A. Faghri, Heat transfer in a pulsating heat pipe with open end. Int. J. Heat Mass Transf. **45**(4), 755–764 (2002). https://doi.org/10.1016/S0017-9310(01)00203-4
16. Y. Zhang, A. Faghri, M.B. Shafii, Analysis of liquid–vapor pulsating flow in a U-shaped miniature tube. Int. J. Heat Mass Transf. **45**(12), 2501–2508 (2002). https://doi.org/10.1016/S0017-9310(01)00348-9
17. R. Lenhard, M. Malcho, J. Jandačka, Modelling of heat transfer in the evaporator and condenser of the working fluid in the heat pipe. Heat Transf. Eng. **40**(3–4), 215–226 (2019). https://doi.org/10.1080/01457632.2018.1426225
18. V. Ayel, L. Araneo, P. Marzorati, C. Romestant, Y. Bertin, M. Marengo, Visualization of flow patterns in closed loop flat plate pulsating heat pipe acting as hybrid thermosyphons under various gravity levels. Heat Transf. Eng. **40**(3–4), 227–237 (2019). https://doi.org/10.1080/01457632.2018.1426244
19. M. Mameli, M. Marengo, S. Zinna, Thermal simulation of a pulsating heat pipe: effects of different liquid properties on a simple geometry. Heat Transf. Eng. **33**(14), 1177–1187 (2012). https://doi.org/10.1080/01457632.2012.677695
20. M. Mohammadi, M. Mohammadi, A.R. Ghahremani, M.B. Shafii, N. Mohammadi, Experimental investigation of thermal resistance of a ferrofluidic closed-loop pulsating heat pipe. Heat Transf. Eng. **35**(1), 25–33 (2014). https://doi.org/10.1080/01457632.2013.810086
21. Z. Gan et al., Experimental study on a hydrogen closed loop pulsating heat pipe with different adiabatic lengths. Heat Transf. Eng. **40**(3–4), 205–214 (2019). https://doi.org/10.1080/01457632.2018.1426223
22. J.L. Xu, Y.X. Li, T.N. Wong, High speed flow visualization of a closed loop pulsating heat pipe. Int. J. Heat Mass Transf. **48**(16), 3338–3351 (2005). https://doi.org/10.1016/j.ijheatmasstransfer.2005.02.034
23. B.Y. Tong, T.N. Wong, K.T. Ooi, Closed-loop pulsating heat pipe. Appl. Therm. Eng. **21**(18), 1845–1862 (2001). https://doi.org/10.1016/S1359-4311(01)00063-1
24. Y.J. Youn, S.J. Kim, Fabrication and evaluation of a slicon-based micro pulsating heat spreader. Sens. Actuators Phys. **174**, 189–197 (2012). https://doi.org/10.1016/j.sna.2011.12.006
25. J. Qu, H. Wu, P. Cheng, Start-up, heat transfer and flow characteristics of silicon-based micro pulsating heat pipes. Int. J. Heat Mass Transf. **55**(21), 6109–6120 (2012). https://doi.org/10.1016/j.ijheatmasstransfer.2012.06.024
26. H.B. Ma, M.A. Hanlon, C.L. Chen, An investigation of oscillating motions in a miniature pulsating heat pipe. Microfluid. Nanofluidics **2**(2), 171–179 (2006). https://doi.org/10.1007/s10404-005-0061-8
27. N. Kammuang-Lue, P. Sakulchangsatjatai, P. Terdtoon, Thermal performance of a closed-loop pulsating heat pipe with multiple heat sources. Heat Transf. Eng. **35**(13), 1161–1172 (2014). https://doi.org/10.1080/01457632.2013.870000
28. S. Arabnejad, R. Rasoulian, M.B. Shafii, Y. Saboohi, Numerical investigation of the performance of a U-shaped pulsating heat pipe. Heat Transf. Eng. **31**(14), 1155–1164 (2010). https://doi.org/10.1080/01457631003689278
29. P. Sakulchangsatjatai, P. Chareonsawan, T. Waowaew, P. Terdtoon, M. Murakami, Mathematical modeling of closed-end pulsating heat pipes operating with a bottom heat mode. Heat Transf. Eng. **29**(3), 239–254 (2008). https://doi.org/10.1080/01457630701756173
30. M.B. Shafii, S. Arabnejad, Y. Saboohi, H. Jamshidi, Experimental investigation of pulsating heat pipes and a proposed correlation. Heat Transf. Eng. **31**(10), 854–861 (2010). https://doi.org/10.1080/01457630903547636
31. N. Kammuang-Lue, P. Sakulchangsatjatai, P. Terdtoon, D.J. Mook, Correlation to predict the maximum heat flux of a vertical closed-loop pulsating heat pipe. Heat Transf. Eng. **30**(12), 961–972 (2009). https://doi.org/10.1080/01457630902837442

32. M. Kumar, R. Kant, A.K. Das, P.K. Das, Effect of surface tension variation of the working fluid on the performance of a closed loop pulsating heat pipe. Heat Transf. Eng. **40**(7), 509–523 (2019). https://doi.org/10.1080/01457632.2018.1436390
33. I.T. Al-Zaharnah, Entropy analysis in pipe flow subjected to external heating. Entropy **5**(5), 391–403 (2003). https://doi.org/10.3390/e5050391
34. I.T. Al-Zaharnah, B.S. Yilbas, Thermal analysis in pipe flow: influence of variable viscosity on entropy generation. Entropy **6**(3), 344–363 (2004). https://doi.org/10.3390/e6030344
35. M. Taghilou, B. Ghadimi, M.H. Seyyedvalilu, Optimization of double pipe fin-pin heat exchanger using entropy generation minimization. Int. J. Eng. **27**(9), 1431–1438 (2014)
36. A. Tandiroglu, Effect of flow geometry parameters on transient entropy generation for turbulent flow in circular tube with baffle inserts. Energy Convers. Manag. **48**(3), 898–906 (2007). https://doi.org/10.1016/j.enconman.2006.08.022
37. O. Mahian, H. Oztop, I. Pop, S. Mahmud, S. Wongwises, Entropy generation between two vertical cylinders in the presence of MHD flow subjected to constant wall temperature. Int. Commun. Heat Mass Transf. **44**, 87–92 (2013). https://doi.org/10.1016/j.icheatmasstransfer.2013.03.005
38. S. Jafarmadar, F. Mobadersani, I. Mirzaee, Investigation of entropy generation through the operation of an unlooped pulsating heat pipe. Int. J. Eng. **29**(8), 1151–1159 (2016)
39. S. Khandekar, A.P. Gautam, P.K. Sharma, Multiple quasi-steady states in a closed loop pulsating heat pipe. Int. J. Therm. Sci. **48**(3), 535–546 (2009). https://doi.org/10.1016/j.ijthermalsci.2008.04.004
40. R. Darby, Correlate pressure drops through fittings. Chem. Eng. **108**(4), 127–127 (2001)
41. F.W. Dittus, L.M.K. Boelter, Heat transfer in automobile radiators of the tubular type. Int. Commun. Heat Mass Transf. **12**(1), 3–22 (1985). https://doi.org/10.1016/0735-1933(85)90003-X
42. A. Bejan, *Convection Heat Transfer* (Wiley, New Jersey, 2013).
43. L. Cheng, 4-Flow Boiling Heat Transfer with Models in Microchannels, in *Microchannel Phase Change Transport Phenomena*. ed. by S.K. Saha (Butterworth-Heinemann, Oxford, 2016), pp. 141–191
44. S. Khandekar, P. Charoensawan, M. Groll, P. Terdtoon, Closed loop pulsating heat pipes part B: visualization and semi-empirical modeling. Appl. Therm. Eng. **23**(16), 2021–2033 (2003). https://doi.org/10.1016/S1359-4311(03)00168-6
45. S. Saitoh, H. Daiguji, E. Hihara, Correlation for boiling heat transfer of R-134a in horizontal tubes including effect of tube diameter. Int. J. Heat Mass Transf. **50**(25), 5215–5225 (2007). https://doi.org/10.1016/j.ijheatmasstransfer.2007.06.019
46. L. Sun, K. Mishima, An evaluation of prediction methods for saturated flow boiling heat transfer in mini-channels. Int. J. Heat Mass Transf. **52**(23), 5323–5329 (2009). https://doi.org/10.1016/j.ijheatmasstransfer.2009.06.041
47. G. Ribatski, J.D. Da Silva, 8-Condensation in Microchannels, in *Microchannel Phase Change Transport Phenomena*. ed. by S.K. Saha (Butterworth-Heinemann, Oxford, 2016), pp. 287–324
48. S. Khandekar, M. Groll, An insight into thermo-hydrodynamic coupling in closed loop pulsating heat pipes. Int. J. Therm. Sci. **43**(1), 13–20 (2004). https://doi.org/10.1016/S1290-0729(03)00100-5
49. A. Cavallini, R. Zecchin, A dimensionless correlation for heat transfer in forced convection condensation. In: Presented at the International Heat Transfer Conference 5, 1974, doi: https://doi.org/10.1615/IHTC5.1220
50. A. Cavallini et al., Condensation in horizontal smooth tubes: a new heat transfer model for heat exchanger design. Heat Transf. Eng. **27**(8), 31–38 (2006). https://doi.org/10.1080/01457630600793970
51. M.K. Dobson, J.C. Chato, Condensation in smooth horizontal tubes. J. Heat Transf. **120**(1), 193–213 (1998). https://doi.org/10.1115/1.2830043
52. K.W. Moser, R.L. Webb, B. Na, A new equivalent reynolds number model for condensation in smooth tubes. J. Heat Transf. **120**(2), 410–417 (1998). https://doi.org/10.1115/1.2824265
53. H. Han, X. Cui, Y. Zhu, S. Sun, A comparative study of the behavior of working fluids and their properties on the performance of pulsating heat pipes (PHP). Int. J. Therm. Sci. **82**, 138–147 (2014). https://doi.org/10.1016/j.ijthermalsci.2014.04.003
54. A. Bejan, *Entropy Generation through Heat and Fluid Flow* (Wiley, New York, 1982).
55. P. Charoensawan, S. Khandekar, M. Groll, P. Terdtoon, Closed loop pulsating heat pipes: part A: parametric experimental investigations. Appl. Therm. Eng. **23**(16), 2009–2020 (2003). https://doi.org/10.1016/S1359-4311(03)00159-5
56. S. Rittidech, P. Terdtoon, M. Murakami, P. Kamonpet, W. Jompakdee, Correlation to predict heat transfer characteristics of a closed-end oscillating heat pipe at normal operating condition. Appl. Therm. Eng. **23**(4), 497–510 (2003). https://doi.org/10.1016/S1359-4311(02)00215-6
57. M.B. Shafii, A. Faghri, Y. Zhang, Thermal modeling of unlooped and looped pulsating heat pipes. J. Heat Transf. **123**(6), 1159–1172 (2001). https://doi.org/10.1115/1.1409266

58. F. Zamzari, Z. Mehrez, A. El Cafsi, A. Belghith, P. Le Quéré, Numerical investigation of entropy generation and heat transfer of pulsating flow in a horizontal channel with an open cavity. J. Hydrodyn. Ser B **29**(4), 632–646 (2017). https://doi.org/10.1016/S1001-6058(16)60776-X
59. K. Esmailpour, B. Bozorgmehr, S.M. Hosseinalipour, A.S. Mujumdar, Entropy generation and second law analysis of pulsed impinging jet. Int. J. Numer. Methods Heat Fluid Flow **25**(5), 1089–1106 (2015). https://doi.org/10.1108/HFF-05-2014-0148
60. T. Tharayil, L.G. Asirvatham, M.J. Dau, S. Wongwises, Entropy generation analysis of a miniature loop heat pipe with graphene–water nanofluid: thermodynamics model and experimental study. Int. J. Heat Mass Transf. **106**, 407–421 (2017). https://doi.org/10.1016/j.ijheatmasstransfer.2016.08.035
61. D. Hacen, K. Slimi, S.B. Nasrallah, Entropy generation for pulsating flow in a composite fluid/porous system. J. Porous Media **11**(6), 557–574 (2008). https://doi.org/10.1615/JPorMedia.v11.i6.40